

A refined empirical line approach for reflectance factor retrieval from Landsat-5 TM and Landsat-7 ETM+

M.S. Moran^{a,*}, R. Bryant^a, K. Thome^b, W. Ni^a, Y. Nouvellon^a, M.P. Gonzalez-Dugo^c,
J. Qi^d, T.R. Clarke^e

^aUSDA Agricultural Research Service, Southwest Watershed Research Center, 2000 East Allen Road, Tucson, AZ 85719, USA

^bOptical Sciences Center Remote Sensing Group, University of Arizona, Tucson, AZ, USA

^cDepartment of Agricultural Engineering, University of Córdoba, Córdoba, Spain

^dDepartment of Geography, Michigan State University, East Lansing, MI, USA

^eUSDA Agricultural Research Service Water Conservation Laboratory, Phoenix, AZ, USA

Received 15 March 2000; received in revised form 10 February 2001; accepted 30 April 2001

Abstract

The recent launch of Landsat-7 ETM+ extends the uninterrupted stream of TM and ETM+ images to a potential span of 32 years. This exceptional image set will allow long-term studies of natural resources, but will require an operational method for converting image digital number (dn) to the temporally comparable surface reflectance factor ($\rho_{s\lambda}$). A refinement to the empirical line (EL) approach for reflectance factor retrieval (RFR) from the Landsat-5 and -7 TM and ETM+ has been proposed. The refined empirical line (REL) approach requires only one within-scene calibration target, minimal field measurements of that target, and a reasonable estimate of dn for $\rho_{s\lambda}=0$ using a radiative transfer model or values provided by this analysis. This study showed that the REL approach worked well for a 10-year Landsat-5 TM and Landsat-7 ETM+ image set in Arizona and $\rho_{s\lambda}$ was retrieved with an estimated accuracy of 0.01. A quantitative approach was proposed to determine the suitability of a within-scene target for the REL approach, and based on historical measurements, a variety of targets met the size and brightness requirements for the REL approach. This operational approach for RFR should encourage long-term investigations of natural resources to answer critical questions regarding resource management and effects of climate changes. © Published by Elsevier Science Inc.

1. Introduction

Landsat Thematic Mapper (TM) sensors have been orbiting the Earth since 1982, providing near-continuous multispectral coverage of the United States every 16 days. The Landsat-4 satellite was launched on July 16, 1982 and continued to acquire TM images into the 1990s. Overlapping the lifespan of the Landsat-4 TM, the Landsat-5 satellite was launched on March 1, 1984 and continued acquiring quality TM images until after the launch of Landsat-7 on April 15, 1999. If Landsat-7 Enhanced Thematic Mapper Plus (ETM+) has a lifespan as long as Landsat-5 TM (~15 years), there will be an uninterrupted legacy of Landsat TM acquisitions spanning 32 years. This excep-

tional temporal coverage, combined with the TM moderate spatial resolution (30 m), reliable geometric integrity, validated radiometric quality, and multispectral range (reflective wavelengths covering the visible, near-infrared, and short-wave infrared), provides the ideal data set for studies of natural resources for improved management.

Such studies will be further facilitated by the current trend to catalog existing TM image archives and make these freely available to noncommercial users upon request. An example is the Water Conservation Laboratory Image and Ground Data Archive produced in 1999 (WIGDA99), which contains 315 entries for spectral images and 709 entries for associated ground data files for an agricultural region and a wildland region in Arizona (Moran, Qi, Ni, & Shannon, 2000). The computer database offers metadata regarding the images and ground data and allows the user to locate data according to user-specified criteria and to determine easily which images are related to which ground data files, and vice versa. In recognition of the importance of such long-term

* Corresponding author. Tel.: +1-520-670-6380 ext. 171; fax: +1-520-670-5550.

E-mail address: moran@tucson.ars.ag.gov (M.S. Moran).

image archives to scientific research, the commercial image providers agreed to waive the company image license agreements for the images in WIGDA99, and to authorize the Water Conservation Laboratory to share the images under a set of reasonable conditions defined by each company.

The most difficult problem in utilizing data sets such as WIGDA99 for studies of temporal change is the fact that TM digital number (dn) is not a good measure of the change in surface conditions over time. That is, dn is a function not only of plant and soil conditions, but also of the sensor calibration, solar zenith angle (θ_s), sensor viewing angle (θ_v), seasonally variable Earth–sun distance, and diurnally variable atmospheric conditions (Slater, 1980). Consequently, for monitoring interannual or even seasonal plant and soil conditions, it is desirable to convert dn to a value that accounts for sensor calibration and is independent of atmospheric and insolation variations. The surface reflectance factor ($\rho_{s\lambda}$ = the ratio of directional reflected to incident radiation at the surface (s) within spectral band λ) is such a value and has become the basic measurement required for most remote sensing algorithms and models.

A generally accepted approach for dn-to- $\rho_{s\lambda}$ conversion (often termed reflectance factor retrieval, RFR) is to measure atmospheric conditions during the satellite overpass with specialized on-site sensors and then use an atmospheric radiative transfer model (RTM) to convert the radiance measurements to surface reflectance factors. Moran, Jackson, Slater, and Teillet (1992) found that using RTMs with on-site atmospheric optical depth and water vapor measurements resulted in $\rho_{s\lambda}$ within ± 0.01 for all TM reflective spectral bands. Though accurate, such methods are often unsuitable for RFR from archived images over a long time span because they require (1) a well-calibrated sensor, (2) comprehensive atmospheric computations through the use of an RTM, and (3) in situ measurements of optical depth on the day of the image acquisition.

These three requirements are not insurmountable, and research and technology development in the last decade has resulted in creative approaches to address or circumvent these issues. First, in response to the need for calibrated sensors, the Landsat TM sensors have been designed to provide on-board calibration and NASA has supported a series of in-flight calibrations over high-reflectance ground targets (e.g., Thome et al., 1993). This has resulted in a good history of the TM sensor calibration with a documented high accuracy. Second, there have been efforts to simplify RTMs to require a minimum number of atmospheric inputs (e.g., Rahman & Dedieu, 1994). Third, there have been numerous approaches proposed to circumvent the need for in situ atmospheric measurements, and, in some cases, to circumvent the need for the RTM altogether. For example, Teillet and Fedosejevs (1995) proposed an approach in which the aerosol optical depth was derived from the RTM using a dark target in the image itself. This approach eliminated the need for atmospheric measurements and yet maintained a high level of RFR accuracy

(estimated to range from 0.01 to 0.033). In an attempt to eliminate the need for both atmospheric measurements and the RTM, others have proposed that an empirical relationship between at-satellite radiance (or dn) and $\rho_{s\lambda}$ based on within-image targets of known $\rho_{s\lambda}$ could be used for RFR with acceptable accuracy. This *empirical line (EL) approach* is the topic of the work presented here.

The EL approach is based on the assumption that within each image, there are at least two targets of low and high reflectance for the spectral bands recorded by the sensor. With the radiances (or dn) extracted from the image and the $\rho_{s\lambda}$ measured (or estimated) for these targets, a linear equation can be developed for RFR (Fig. 1a). This equation will account for both illumination and atmospheric effects and can be applied to the remotely sensed data to produce images in units of $\rho_{s\lambda}$ (Smith & Milton, 1999). In practice, the EL approach is implemented in a variety of ways with the most monumental tasks being the selection of calibration targets and the determination of target $\rho_{s\lambda}$. When suitable bright and dark targets were not available, a linear relation between dn and $\rho_{s\lambda}$ has been derived from a single bright target, assuming surfaces of zero reflectance will produce zero radiance. The accuracy of the single-target EL approach

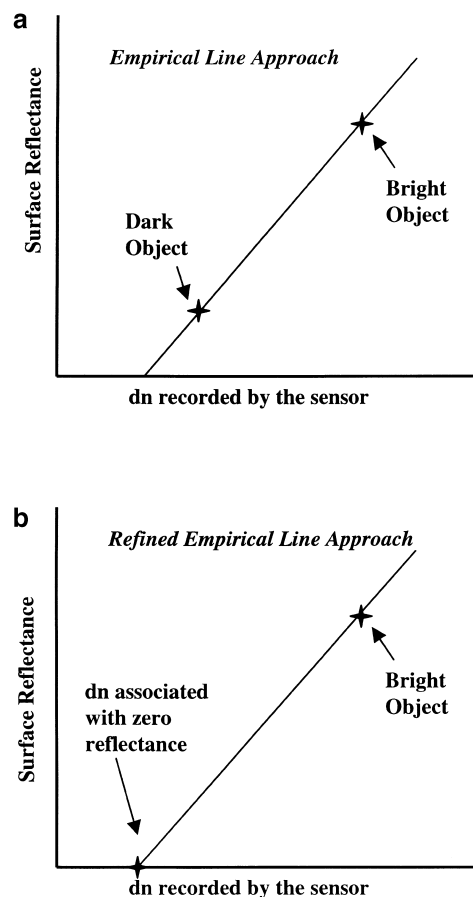


Fig. 1. The derivation of the prediction equation (a) from two within-image calibration targets for the EL approach and (b) from one within-image target and a modeled dn for $\rho_{s\lambda} = 0$ for the REL approach.

has been reported to be relatively poor, with reported errors in RFR of 15–20% (Freemantle, Pu, & Miller, 1992; McCardle, Miller, & Freemantle, 1992). On the other hand, when dark and bright targets are available and well characterized, the reported accuracy is better than 10% and depends almost exclusively on the accuracy of the characterization of the calibration targets (Caselles & López García, 1989; Schott, Salvaggio, & Volchok, 1988).

A refinement of the EL approach, termed refined empirical line (REL) approach, is proposed, which resolves some of the difficulties of the conventional EL approach and includes the advantages of the RTM-based approaches. The REL approach derives the relation between dn and $\rho_{s\lambda}$ based on two points: a single high-reflectance target within the scene and an estimate of the image dn that would be associated with a surface of $\rho_{s\lambda} = 0$ (Fig. 1b). The estimate of dn for $\rho_{s\lambda} = 0$ is obtained through the use of an RTM with reasonable water and aerosol models, or measurements of atmospheric conditions on a *typical* cloud-free day. The accuracy of RFR using the REL approach is largely dependent upon accurate estimations of $\rho_{s\lambda}$ of the bright calibration target and dn for $\rho_{s\lambda} = 0$. Thus, the main issues addressed in this study are:

1. selection of a calibration target;
2. characterization of the $\rho_{s\lambda}$ of the calibration target; and
3. computation of dn for $\rho_{s\lambda} = 0$.

The method for characterization of the $\rho_{s\lambda}$ of the calibration target can be accomplished in a half day and accounts for variations in sun/sensor/target geometry. The method for computation of dn for $\rho_{s\lambda} = 0$ is based on atmospheric measurements made on any date at the location, or reasonable estimates of atmospheric conditions at the location. The basic idea of the REL approach is that the half-day effort to accurately characterize $\rho_{s\lambda}$ of a single site will allow for the relative inaccuracy associated with the estimate of dn for $\rho_{s\lambda} = 0$, resulting in an operational RFR method of suitable accuracy that requires only one high-reflectance target. Furthermore, due to the proposed target characterization, we will show that the target need not necessarily meet the requirement of most EL approaches to be Lambertian and free of vegetation.

Implementation of the REL approach is reported in the next sections based on data derived from WIGDA99 at two Arizona field sites: Maricopa Agricultural Center (MAC; an agricultural region) and the Walnut Gulch Experimental Watershed (WGEW; a semiarid rangeland). The accuracy of RFR using the REL approach will be demonstrated for Landsat-5 and Landsat-7 TM images of WGEW over a 10-year period.

2. Experimental design and methods

This section provides a short description of the field experiments that are related to this REL demonstration and

the standard methods that were used to measure surface and atmosphere conditions during Landsat TM and TM simulator overpasses.

2.1. Experiments

MAC is located about 48 km south of Phoenix, AZ, in an extensive irrigated agricultural region, and is composed of large fields (up to 0.3×1.6 km) used for demonstrating new farming techniques on a production scale. WGEW is located in SE Arizona in a semi-arid region characterized by grass brush rangeland and is the most well-instrumented, semi-arid watershed in the world (Renard et al., 1993). Both MAC and WGEW have been the sites for several multi-disciplinary field experiments that focused on studies of multi-spectral remote sensing for evaluation of soil, plant, and atmospheric conditions (Goodrich et al., 2000; Jackson, 1990; Kustas & Goodrich, 1994; Moran, Clarke, Qi, & Pinter, 1996; Moran, Goodrich, & Kustas, 1994).

The MAC experiments were a series of large-scale field experiments to study ground-, aircraft- and satellite-based remote sensing of agricultural crops and soils. These were “brown bag” experiments in which all participants provided their own funds and all shared their data with other participants. Similar experiments, some with NASA funding, were conducted at WGEW. Short descriptions of the experiments related to this research are included in Table 1.

2.2. Measurement of surface reflectance factor

From 1984 to the present, $\rho_{s\lambda}$ of large targets at MAC and WGEW has been measured according to the following methodology. From 1984 to the present, $\rho_{s\lambda}$ has been measured with four-band Exotech radiometers with TM filters (TM spectral bands 1–4) and the eight-band Modular Multispectral Radiometer (MMR) simulating all seven TM spectral bands. The reference reflectance standard has been a $2' \times 2'$ BaSO₄ or molded halon plate that was calibrated frequently for absolute reflectance and non-Lambertian properties (Jackson, Moran, Slater, & Biggar, 1987). For ground-based measurements, the Exotech or MMR radiometers were mounted in backpack-like yokes that held the sensor in a nadir-looking position about 2 m above the surface and 1 m from the right shoulder of the operator. Thus, the operator could make a multitude of measurements along designated transects, and return to make frequent measurements of the reference plate. During most Landsat overpasses at MAC and WGEW, yoke-based measurements of $\rho_{s\lambda}$ over a 480×120 m (16×4 TM pixels) target were completed within a 20-min interval.

It was also possible to measure $\rho_{s\lambda}$ over larger areas by mounting the Exotech radiometer in an aircraft and making continuous measurements along known transects at MAC and WGEW. The Exotech was fitted with 15° FOV lenses and flown at 50–100 m AGL resulting in a measurement footprint of approximately 15–25 m (comparable to a TM

Table 1
Short descriptions of the experiments at MAC and WGEW related to this research

Project name	Description
MAC SPOT	A season-long experiment designed to test satellite-based remote sensing for real-time farm management. We acquired 17 SPOT HRV images (viewing angles +24 to -28; XS and Pan) and 13 Landsat TM images from April through October 1989.
MADMAC	The Multispectral Airborne Demonstration at MAC (MADMAC) was designed to test the potential of remote sensing information for farm management applications through analysis of a season-long set of high-resolution (2 m pixel) multispectral videographic images with detailed supporting ground measurements. Fourteen images acquired with a multispectral video camera system covering the visible-, near-, and thermal-infrared spectrum from Utah State University were acquired biweekly at 2- and 4-m resolution from April through September 1994.
MAC ATLAS	In cooperation with NASA Stennis Space Center, images from the Airborne Terrestrial Applications Scanner (ATLAS) were obtained throughout a single cotton growing season, with 15 spectral bands (visible to thermal), 2.5 m ground resolution, 72 FOV. Extensive ground-based measurements of surface reflectance, temperature, and crop and soil conditions were made during each overpass.
Monsoon'90	The Monsoon'90 multidisciplinary field campaign was conducted at the USDA ARS Walnut Gulch Experimental Watershed (WGEW) in SE Arizona during June–September 1990. The objective of this combined ground, aircraft, and satellite campaign was to assess the feasibility of utilizing remotely sensed data coupled with water and energy balance modeling for large area estimates of fluxes in semiarid rangelands.
WG'92	The Walnut Gulch'92 field campaign was conducted during the dry, early-monsoon, mid-monsoon, post-monsoon and “drying” seasons from April through November 1992 at WGEW. The overall research goal was to investigate the seasonal hydrologic dynamics of the region and to define the information potential of combined optical microwave remote sensing.

pixel). A second Exotech radiometer was cross-calibrated with the airborne Exotech and then mounted over a reference plate to make measurements every 1–5 min. The plate measurements were multiplied by the instrument cross-calibration and used to convert the measurements made with the airborne radiometer to $\rho_{s\lambda}$. The flight altitude of <100 m AGL was chosen to minimize atmospheric effects on measurement of $\rho_{s\lambda}$; Moran et al. (1995) reported that the difference between yoke- and aircraft-based $\rho_{s\lambda}$ was less than 0.005 for all TM spectral bands. At MAC, the aircraft-based approach was used to measure $\rho_{s\lambda}$ along transects through the center of the large fields (1.6 × 0.3 km). At WGEW, two transects were surveyed to intersect two meteorological/flux stations including the major plant groups and soil types in the watershed at eight study targets.

To measure the bidirectional reflectance factor as a function of sensor viewing angle (θ_v), an Exotech radiometer was mounted on a 2.5-m swinging boom that allowed $\rho_{s\lambda}$ of a target of approximately 0.5 m diameter to be measured over the range of $-45^\circ < \theta_v < 45^\circ$ at 5° increments. Results from these measurements have been used to determine the surface bidirectional reflectance distribution function (BRDF) through simulation models for bare soils and plant canopies (Qi, Cabot, Moran, Dedieu, & Thome, 1995; Qi, Moran, Cabot, & Dedieu, 1995). The general approach is to use the yoke-based measurements over a large target for an assessment of the absolute $\rho_{s\lambda}$, and use the boom-based device to determine the shape of the relation between $\rho_{s\lambda}$ and θ_v (Jackson et al., 1990).

2.3. Conventional RFR from satellite-based images

Procedures to retrieve $\rho_{s\lambda}$ using satellite-based sensors must account for the absorption and scattering of radiation through the atmosphere. Commonly, RFR from satellite-based images is achieved by measuring atmospheric optical depth, gaseous transmittance, and water vapor absorption during the overpass and using a RTM to compute at-satellite radiance (L_λ) for several assumed values of $\rho_{s\lambda}$.

A linear relation between L and $\rho_{s\lambda}$ over the range of $\rho_{s\lambda} = 0.01–0.7$ can be used with the sensor absolute radiance calibration to retrieve $\rho_{s\lambda}$ from satellite-based images (Slater & Jackson, 1982). Accuracies of $\rho_{s\lambda}$ retrieved with this approach are generally reported to be on the order of $\pm 5\%$ (Slater et al., 1987).

In cooperation with scientists from the University of Arizona Optical Science Center, this RFR approach was implemented many times during Landsat overpasses at MAC and WGEW. A sun photometer was deployed on site from near sunrise until solar noon. Atmospheric effects on the days of overpasses were characterized by Langley plot measurements to determine total spectral optical depths, which were partitioned into Mie, Rayleigh, and ozone optical depths (Biggar, Gellman, & Slater, 1990). Gaseous transmittance was estimated using the 5S radiative transfer code (Tanré et al., 1990) and columnar water vapor was measured for correction for water vapor absorption. Values of optical depth were used as inputs to an RTM (Herman & Browning, 1965) to compute the relation between $\rho_{s\lambda}$ and L_λ . An inversion of this approach, with refinements over time, is currently used over bright surfaces (e.g., White Sands) for in-flight sensor calibrations of Landsat TM and ETM+ sensors (Thome et al., 1993).

3. Application of the REL approach

The three issues addressed in this study of the REL approach are (1) selection of a calibration target; (2) characterization of the $\rho_{s\lambda}$ of the calibration target; and (3) computation of dn for $\rho_{s\lambda} = 0$. The following subsections offer analysis of these issues and suggestions for REL implementation.

3.1. Selection of REL calibration target

Selection of the calibration target has been the topic of several studies. For RFR from aircraft-based sensors, tar-

gets have included roofs (Moran, Clarke, Qi, Barnes, & Pinter, 1997), roads (Freemantle et al., 1992), and water tanks (McCardle et al., 1992). Smith and Milton (1999) suggested that the target should be (1) large, (2) near-Lambertian, and (3) devoid of vegetation. Since the REL approach includes the use of a BRDF model for site characterization (see Section 3.2), the target selection criteria should simply include (1) large size, (2) high reflectance, and (3) stability of BRDF over time. The target size is directly related to the sensor spatial resolution and radiometric quality and to other site-specific factors such as atmospheric conditions and the contrasting reflectance of surrounding surfaces. That is, if atmospheric scattering is high and the calibration target is a dark surface surrounded by a bright surface, it would be prudent to select a target large enough to ensure a number of pixels uncontaminated by atmospheric adjacency effect (Slater, 1980). Moran et al. (1997) showed that for a bright target surrounded by a darker surface under extremely clear atmospheric conditions, it was still necessary to have a ratio of sensor resolution to target size of 1:8 to ensure that at least four pixels remain uncontaminated in the center of the bright target. Using this criteria for the Landsat TM sensor with a 30-m resolution, the minimum target size would be 240×240 m. Assuming that there is a target of sufficient size and brightness within the image, the only remaining selection criterion is stability of BRDF over time.

Using the temporal measurements of surface reflectance in the WIGDA99 data set, it was possible to assess the stability of a number of potential calibration targets at MAC and WGEW. The stability of the BRDF of each target was assessed based on the relation between $\rho_{s\lambda}$ and θ_s and sensor view azimuth and zenith angles (ϕ and θ_v , respectively). An example of a simple empirical BRDF equation is that proposed by Walthall, Norman, Welles, Campbell, and Blad (1985) and modified by Nilson and Kuusk (1989):

$$\rho = K_0 + K_1\theta_s\theta_v\cos\phi + K_2\theta_s^2\theta_v^2 + K_3(\theta_s^2 + \theta_v^2), \quad (1)$$

where K_0 , K_1 , K_2 , and K_3 are empirical parameters. For a nadir-looking sensor like Landsat TM and ETM+, the relation simplifies to a function of θ_s , where:

$$\rho = K_0 + K_3\theta_s^2. \quad (2)$$

Thus, the suitability of the potential calibration target can be assessed by determining the relation between $\rho_{s\lambda}$ and θ_s and computing the mean absolute difference (MAD) between the modeled and measured values. A site with good potential for REL calibration would have a low MAD for all wavelengths, indicating that $\rho_{s\lambda}$ was a function of θ_s and target surface variability was minimal. A summary of our findings is presented in Sections 3.1.1 and 3.1.2. In Section 3.1.3, other issues affecting the $\rho_{s\lambda}$ stability, such as surface moisture condition due to water table variations and precipitation, are addressed.

3.1.1. Calibration targets: agricultural site

During 1989 MACSPOT, and again during 1994 MAD-MAC, we measured the reflectance of a rough, bare soil field throughout the experiment with an aircraft-based Exotech radiometer in 1989 and a yoke-based Exotech radiometer in 1994, with TM spectral bands. This resulted in 22 measurements from day of year (DOY) 99 to 297 in 1989 in MAC field 17, and 41 measurements from DOY 147 to 271 in 1994 in field 10. According to field notes, these fields were left unmolested throughout the experiment. The measurements of $\rho_{s\lambda}$ and θ_s for both fields illustrate relations that are typical for a rough, non-Lambertian surface and can be characterized by Eq. (2) (Fig. 2a and b). The scatter from the modeled relation is likely due to basic errors in measurement of $\rho_{s\lambda}$ (estimated to be ± 0.01 by Slater et al., 1987) and the effects of pitch, yaw, and roll of the aircraft. The MAD of the modeled and measured values was less than or equal to 0.012 for TM spectral bands 1–4 (Table 2). Some drawbacks to using rough bare soil targets are (1) the relatively low value of $\rho_{s\lambda}$ ranging from about 0.1 to 0.4 for TM spectral bands 1–4 and (2) the gradual brightening of the target over a season due to rain compaction.

Another potential calibration target in agricultural regions with high $\rho_{s\lambda}$ in the NIR spectrum is a cropped field of 100% vegetation cover. During the 1989 MAC-SPOT experiment, we measured $\rho_{s\lambda}$ of irrigated alfalfa and cotton fields. Based on field notes, we selected only the measurements made when the alfalfa and cotton were greater than 90% cover, resulting in 8 days for alfalfa and 7 days for cotton. The $\rho_{s\lambda}$ of the alfalfa fields with cover $\geq 90\%$ had a weak relation with θ_s (MAD=0.054 for TM spectral band 4; Fig. 2c) due most likely to the fact that alfalfa in Arizona does not achieve a high green leaf area index (GLAI) before it is harvested. In contrast, the $\rho_{s\lambda}$ of the cotton field stayed fairly constant (at about 0.6 $\rho_{s\lambda}$ in TM spectral band 4) over the 42-day period of interest (MAD=0.013 for TM spectral band 4; Fig. 2d). The GLAI of mature cotton can be as high as 6.0, whereas the GLAI of mature alfalfa in Arizona rarely exceeds 2.0. Thus, based on this analysis, a cropped field of high GLAI would have potential as a high-reflectance calibration target for the NIR wavelength range.

Finally, many agricultural regions have packed earth roads, parking lots, and landing strips that have potential for calibration targets. During 1998 MAC-ATLAS, yoke-based measurements of $\rho_{s\lambda}$ of a packed earth parking lot were made throughout the morning on 5 days, resulting in 21 measurements. The $\rho_{s\lambda}$ had a strong cosine relation with θ_s for all TM spectral bands over a large range of θ_s values, resulting in MAD between measured and modeled $\rho_{s\lambda}$ of less than 0.01 for TM spectral bands 1–4 (Fig. 2e, Table 2). Similar results were found for a paved parking lot and a packed earth parking lot at WGEW (not shown here). One advantage of using packed earth targets for REL is the generally high reflectance of such targets which, in this case, ranged from ~ 0.20 to 0.50 for TM spectral bands 1–4.

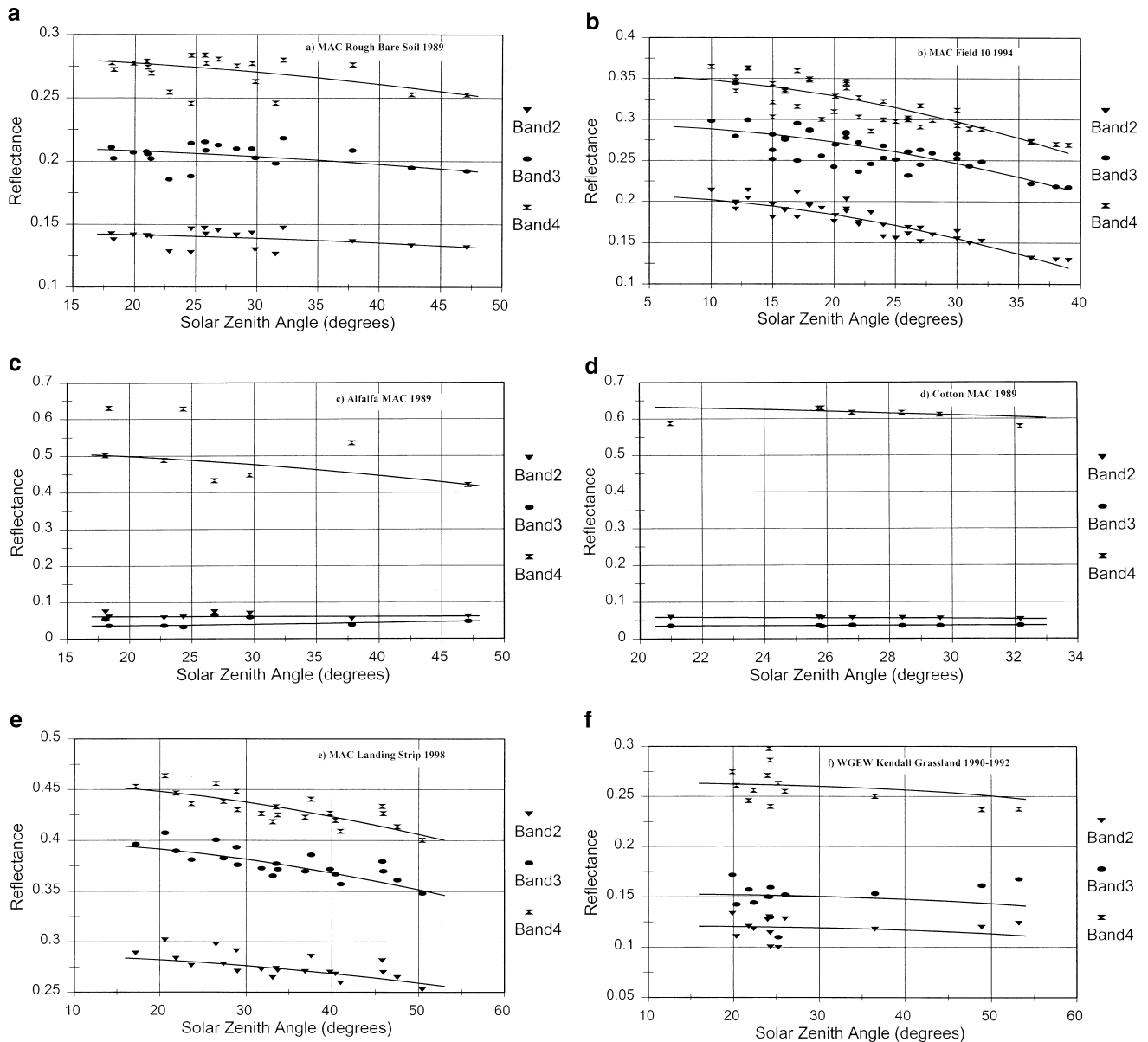


Fig. 2. The measured (solid symbols) and modeled (solid line) values of $\rho_{s\lambda}$ and θ_s for (a–b) rough bare soil fields at MAC, (c) MAC alfalfa, (d) MAC cotton, (e) MAC packed earth landing strip, and (f) WGEW Kendall grassland. The legend captions Band2, Band3, and Band4 refer to the Landsat-5 TM spectral bands 2 (green), 3 (red), and 4 (NIR); results for TM spectral band 1 (blue) were similar to results for band 2 and were omitted for figure clarity.

In summary, of the common agricultural targets available for REL calibration, the best sites would be rough bare soil surfaces and packed earth roads or parking lots. Vegetated targets could be used for the NIR wavelength spectral bands, but only when the GLAI was very high, as in the case of mature, irrigated cotton.

3.1.2. Calibration targets: rangeland site

During the Monsoon'90 and WG'92 experiments, the reflectance of a 0.2×0.5 km semi-arid grassland target was measured repeatedly on 13 dates during the dry and monsoon seasons. Over this 3-year period, with measurements made in April through October, the grassland GLAI ranged from zero to 1.0. With such low GLAI, there was potential

for the soil reflectance to dominate the total reflectance, thus allowing the grassland target to be used for REL calibration. Results showed that the correlation with θ_s was weak, and the modeled values differed from measured values, with MAD values as high as 0.028 for TM spectral band 4 (Fig. 2f, Table 2). The scatter was likely due to the changes in vegetation biomass associated with seasonal grassland growth. These results are discouraging for the use of sites with sparse, yet variable, vegetation for REL calibration.

Within WGEW, there is a relatively flat 0.3×0.3 km area of packed earth associated with a nearby mining activity (hereafter referred to as the WGEW mine target) that has remained unmolested for over a decade. There was no historical record of $\rho_{s\lambda}$ for this site, so throughout a single

Table 2

The MAD of the modeled and measured values of $\rho_{s\lambda}$ for calibration targets at MAC and WGEW for TM spectral bands 1–4 (labeled Band1, Band2, Band3, and Band4), related to Figs. 2–4

Location	<i>n</i>	Band1	Band2	Band3	Band4
MAC Bare Soil 1989	22	0.004	0.005	0.006	0.009
MAC Field 10 1994	8	0.006	0.007	0.012	0.013
MAC Alfalfa 1989	7	0.006	0.006	0.009	0.054
MAC Cotton 1989	21	0.002	0.001	0.001	0.013
MAC Landing Strip 1998	41	0.006	0.007	0.007	0.008
Kendall 1990/1992	13	0.010	0.013	0.015	0.028
WGEW Mine	5	0.003	0.004	0.004	0.003
White Sands	15	0.034	0.035	0.036	0.037

morning on July 1, 1999, a series of yoke-based measurements of $\rho_{s\lambda}$ was made over an area of 4×4 Landsat-7 ETM+ 30-m pixels within the mine target. The results showed a good correlation with θ_s over a range from 20° to 50° with a MAD between measured and modeled values of less than 0.01 for TM spectral bands 1–4 (Table 2, Fig. 3a). This good relation was achieved despite the internal heterogeneity of the mine target, as illustrated by the large standard deviation of $\rho_{s\lambda}$ measurements for the 16 pixels at the five θ_s . These results support the concept that a good REL calibration target should be spectrally invariant over time, but not necessarily of uniform reflectance. With such heterogeneous targets, it will be critical to have high precision in the geolocation of the target to ensure that the same location is extracted from all images for REL calibration.

3.1.3. Other considerations

It has been emphasized here that a characteristic of an REL calibration target is an invariant BRDF over time. Two surface conditions that can affect BRDF invariance are changes in vegetation biomass (as illustrated in Fig. 2f) and changes in surface soil moisture. The latter issue is the topic of this subsection. Surface soil moisture varies with the intensity and recency of rainfall, and, in some cases, variations in water table height. At the WGEW mine site, we conducted a simulation of the effects of precipitation on $\rho_{s\lambda}$ by sprinkling the surface of the WGEW mine target at WGEW with enough water to saturate the surface to a depth of 2 cm. Measurements made before and after saturation showed that for this July date at 10:00 MST with cloud-free conditions and moderate winds, $\rho_{s\lambda}$ decreased substantially with increased soil moisture but returned to the pre-application $\rho_{s\lambda}$ within 15 min (Fig. 3b). Considering that images of interest for temporal analysis are generally selected with cloud-free conditions, the effects of precipitation on characterized REL targets would be minimal for this location. Continuing investigation and characterization of such targets and quantification of the effects of precipitation should be a component of REL research.

Fluctuating water tables are another concern in selection of REL calibration targets. Previous studies on the EL

approach have suggested that desert surfaces such as alkali flats would provide a smooth, extensive, bare area for calibration (Smith & Milton, 1999). Such an area that might be considered is White Sands, NM, which has been the site for numerous field campaigns for in-flight absolute calibration of the Landsat TM, ETM+, and other sensors (Thome et al., this issue, 1993). An analysis of $\rho_{s\lambda}$ measured for the University of Arizona calibration target at White Sands for 15 dates from 1987 to 1992 showed a great deal of variability in $\rho_{s\lambda}$, with a MAD between measured and modeled values as high as 0.037 for TM spectral band 4 (Fig. 4). The White Sands calibration target is bright and flat, but is characterized by a shallow, fluctuating water table. This does not decrease its value as an in-flight vicarious calibration site, but it would not be appropriate as an REL calibration target.

3.2. Characterization of REL calibration target

The procedure proposed for characterization of the REL calibration target is based on a methodology originally refined for satellite sensor in-flight calibration at White Sands, NM, by Jackson et al. (1990). The REL procedure requires sets of target $\rho_{s\lambda}$ measured over a variety of θ_s and θ_v . This can be accomplished in a single morning starting near dawn and finishing near solar noon. The two sets of measurements are made with a yoke-based sensor and

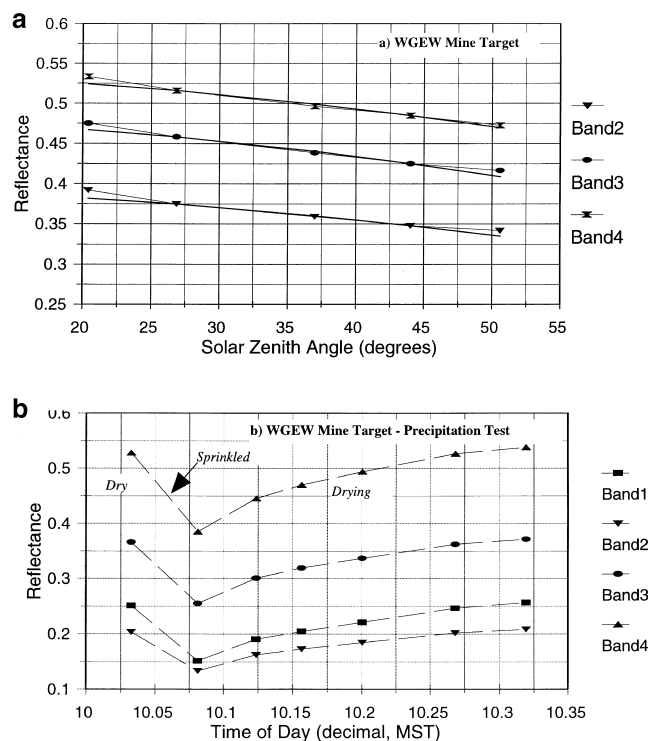


Fig. 3. (a) The measured (solid symbols) and modeled (solid line) values of $\rho_{s\lambda}$ and θ_s for a disturbed area associated with a mine in WGEW, where Band2, Band3, and Band4 refer to the Landsat-5 TM spectral bands 2 (green), 3 (red), and 4 (NIR). (b) Temporal measurements of $\rho_{s\lambda}$ from a dry, packed earth surface, which was subsequently wetted to 2 cm, and allowed to air-dry.

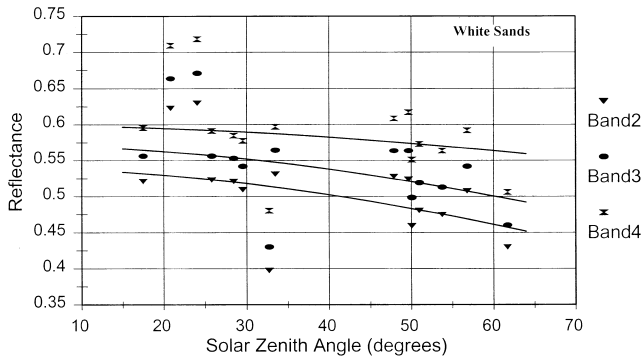


Fig. 4. The measured (solid symbols) and modeled (solid line) values of $\rho_{s\lambda}$ and θ_s for a calibration target at White Sands, NM, where Band2, Band3, and Band4 refer to the Landsat-5 TM spectral bands 2 (green), 3 (red), and 4 (NIR).

another sensor mounted on a swinging boom, as described previously. The yoke-based sensor can be deployed to measure $\rho_{s\lambda}$ over the entire area of interest at frequent intervals to produce a data set similar to that presented in Fig. 3a. The sensor mounted on the swinging boom can be deployed to measure $\rho_{s\lambda}$ at a single representative point within the target for multiple θ_s and θ_v . An example of such measurements for the WGEW mine target is presented in Fig. 5. In the principal plane of the sun, rough nonspecular targets will generally reflect highest at the hot spot (the geometry in which $\theta_s = \theta_v$) and lower in the forward-than back-scattering direction. In the orthogonal plane of the sun, $\rho_{s\lambda}$ will have a symmetric relation with θ_v , forming a slightly convex or concave shape.

The yoke-based measurements provide the relation between target $\rho_{s\lambda}$ and θ_s , and the boom-based measurements provide the shape of the relation between target $\rho_{s\lambda}$ and θ_v . These measurements can be used as input to a simple empirical BRDF model (such as Eq. (1)) to compute the BRDF of the calibration target. Using measurements of the WGEW mine, we computed the mine BRDF using the SOILSPECT model (Jacquemund, Baret, & Hanocq, 1992) and produced the mine BRDF. It should be emphasized that with the Landsat sensors' field of view of $\pm 7.5^\circ$, there is minimal error associated with variations in ϕ and θ_v and REL calibration targets could be characterized simply with a relation between $\rho_{s\lambda}$ and θ_s such as Eq. (2).

3.3. Computing the dn associated with $\rho_{s\lambda} = 0$

In the REL approach, the second point required to compute a relation between $\rho_{s\lambda}$ and dn is the dn associated with $\rho_{s\lambda} = 0$. This value can be derived through the use of an RTM with a standard atmosphere suitable for the geographic location or with atmospheric measurements made on site during typical atmospheric conditions. The RTM can provide an estimate of at-satellite radiance for $\rho_{s\lambda} = 0$, which can be converted to Landsat TM dn using the TM absolute calibration coefficients. Landsat-4 and -5 TM calibration

coefficients have been reported throughout the lifetimes of the sensors (Slater et al., 1987; Thome et al., 1993) and have been validated for RFR at other locations of low and high reflectance (Moran et al., 1992). Recently, results from an in-flight calibration of the Landsat-7 ETM+ sensor were reported by Thome et al. (this issue). These Landsat-7 ETM+ calibration coefficients were used with on-site atmospheric measurements and an RTM (as described above) to retrieve $\rho_{s\lambda}$ from the ETM+ images of MAC and WGEW. The retrieved $\rho_{s\lambda}$ were compared with ground-based measurements of $\rho_{s\lambda}$ of a uniform bare soil field at MAC (0.8×0.2 km) and the Kendall grassland site (0.12×0.5 km) in WGEW (Fig. 6). This is an independent validation on the ETM+ calibration results reported by Thome et al. and shows that $\rho_{s\lambda}$ was retrieved with a MAD between measured and retrieved values of less than 0.035 for ETM+ spectral bands 1–4, respectively. The accuracy of in-flight calibrations over bright targets is generally reported to be on the order of 5%. The mean percentage difference of the results at MAC and WGEW for ETM+ spectral bands 1–4 was 7.1%, thus instilling confidence in the use of the Landsat-4 and -5 TM and Landsat-7 ETM+ published calibration coefficients for the REL approach for multitemporal studies.

Using the WGEW and MAC as examples, we compiled a set of RTM outputs at MAC and WGEW over the past 10 years for dates when Landsat TM and ETM+ images

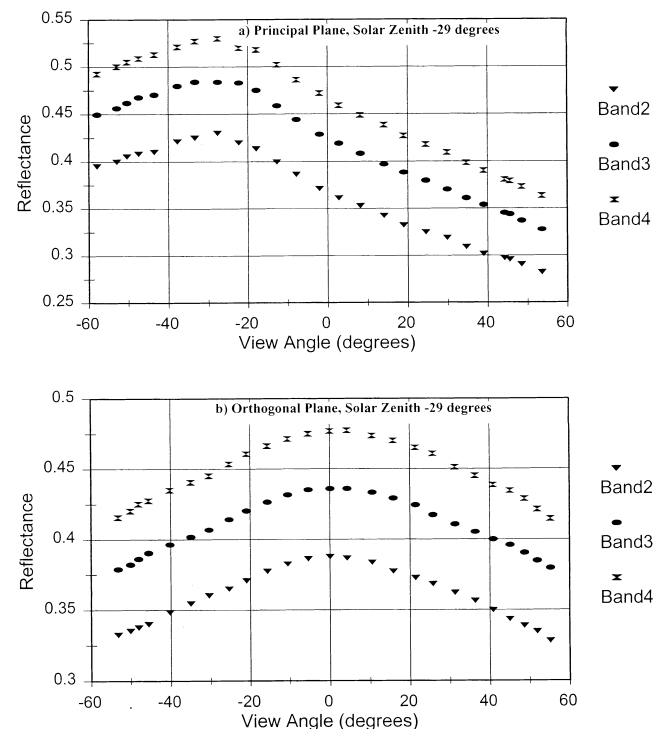


Fig. 5. The measured (solid symbols) values of $\rho_{s\lambda}$ and θ_v for the WGEW mine target in (a) the principal plane and (b) the orthogonal plane, where Band2, Band3, and Band4 refer to the Landsat-5 TM spectral bands 2 (green), 3 (red), and 4 (NIR).

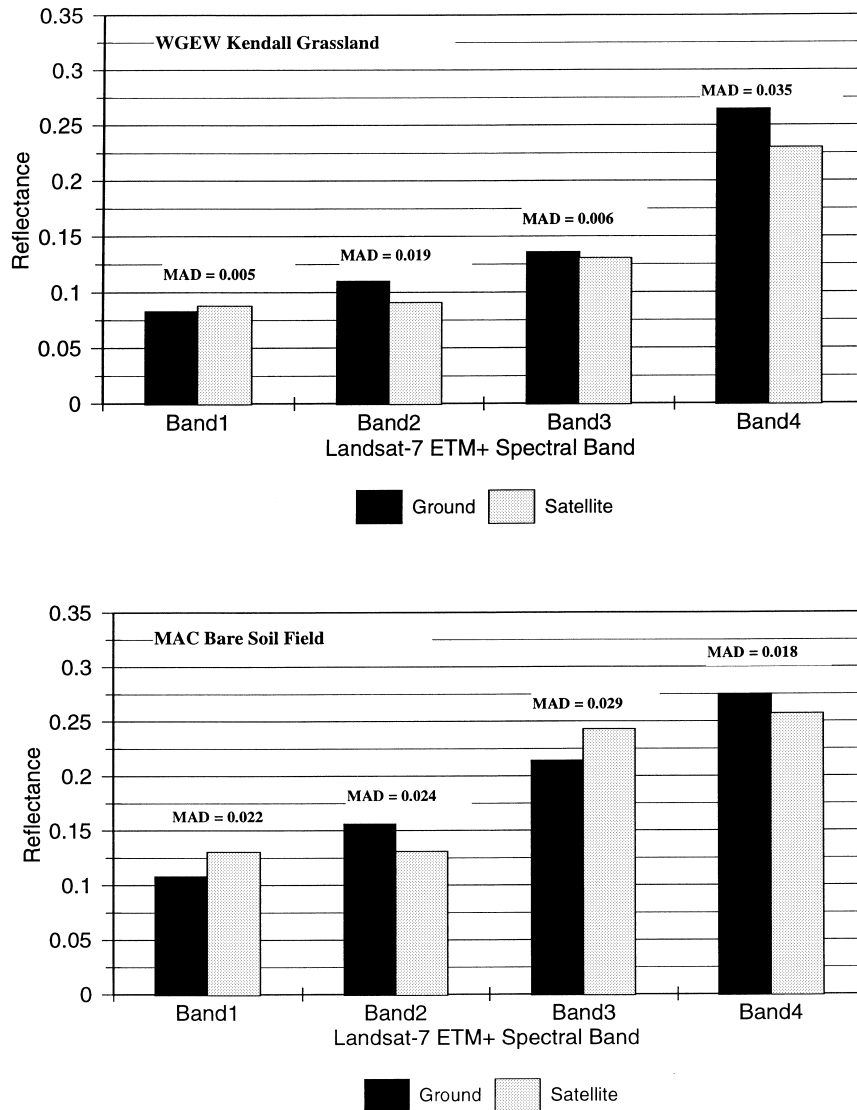


Fig. 6. Values of $\rho_{s\lambda}$ retrieved from the Landsat-7 ETM+ image using conventional atmospheric measurements and an RTM compared with ground-based measurements of $\rho_{s\lambda}$ of a uniform bare soil field at MAC and the Kendall grassland site in WGEW, where Band2, Band3, and Band4 refer to the Landsat-7 ETM+ spectral bands 2 (green), 3 (red), and 4 (NIR).

were obtained with less than 10% cloud cover and clouds did not occlude the path of the sun at overpass time. The RTM output, based on on-site atmospheric measurements as described previously, provided the estimate of at-satellite radiance for $\rho_{s\lambda} = 0$. This was converted to Landsat TM and ETM+ dn and the averages of all dn in each TM spectral band were assumed to be the best estimate of dn for $\rho_{s\lambda} = 0$ at WGEW and MAC (Table 3). The range of optical depths and gaseous transmittance associated with the results presented in Table 3 are listed in Table 4.

4. Validation of the REL approach

The REL approach was implemented using a 10-year archive of Landsat-5 TM and Landsat-7 ETM+ images of

WGEW, the ground-based measurements of $\rho_{s\lambda}$ of the WGEW mine target, and a history of atmospheric measurements and RTM output for WGEW. The results of the REL approach were validated with independent measurements of $\rho_{s\lambda}$ of the Kendall grassland on four dates over 7 years for Landsat-5 TM (September 9, 1990, September 4, 1991, October 2, 1992, and March 20, 1997) and one date (September 26, 1999) for Landsat-7 ETM+. The dn-to- $\rho_{s\lambda}$ relation for WGEW for each date was computed based on two points: the extracted dn for the mine target and the mine $\rho_{s\lambda}$ determined by the BRDF equation derived for the mine, and the average dn for $\rho_{s\lambda} = 0$ at WGEW from Table 3. For each of the five dates, $\rho_{s\lambda}$ was retrieved from the Landsat-5 or -7 scenes for the Kendall site and compared with the measured $\rho_{s\lambda}$. Results showed that the MAD between retrieved and measured $\rho_{s\lambda}$ was less than or equal to 0.01 for TM spectral

Table 3

The Landsat TM and ETM+ dn for $\rho_{s\lambda} = 0$ at WGEW and MAC for TM and ETM+ spectral bands 1–4 (labeled Band1, Band2, Band3, and Band4), estimated from an RTM with inputs based on on-site measurements of atmospheric conditions

Date	Band1	Band2	Band3	Band4
<i>MAC, Landsat-5 TM</i>				
May 31, 1985	46	14	10	5
August 8, 1985	55	17	13	6
April 21, 1986	48	14	10	5
June 24, 1986	55	17	13	6
July 26, 1992	46	14	11	5
Average (S.D.)	50 (4)	15 (1)	11 (1)	6 (1)
<i>WGEW, Landsat-5 TM</i>				
June 5, 1990	45	14	10	5
April 23, 1992	45	14	11	6
June 10, 1992	31	14	11	6
July 12, 1992	43	13	10	6
August 13, 1992	45	14	11	6
September 30, 1992	38	12	9	5
November 1, 1992	36	11	9	5
November 17, 1992	33	11	8	5
Average (S.D.)	40 (13)	13 (4)	10 (3)	6 (2)
<i>MAC, Landsat-7 ETM+</i>				
September 24, 1999	60	29	40	19
<i>WGEW, Landsat-7 ETM+</i>				
September 26, 1999	50	33	24	18

bands 1–4 (Fig. 7). Such accuracy is suitable for most algorithms and models that are used to derive data products for agricultural and grassland resource management.

The sensitivity of the REL approach to the selection of the dn for $\rho_{s\lambda} = 0$ was tested by recomputing the REL slope and offset for the Landsat-5 TM WGEW scenes using the minimum and maximum dn values rather than the average

Table 4

The range of aerosol and Rayleigh optical depth and total gaseous transmittance derived from on-site atmospheric measurements for the dates listed in Table 3, where TM and ETM+ spectral bands 1–4 are labeled Band1, Band2, Band3, and Band4

	Band1	Band2	Band3	Band4
<i>MAC</i>				
Maximum aerosol optical depth	0.1785	0.1458	0.1212	0.0926
Minimum aerosol optical depth	0.0578	0.0478	0.0401	0.0301
Maximum Rayleigh optical depth	0.1548	0.0806	0.0444	0.0170
Minimum Rayleigh optical depth	0.1540	0.0802	0.0442	0.0169
Maximum gaseous transmittance	0.9901	0.9421	0.9559	0.9683
Minimum gaseous transmittance	0.9860	0.9200	0.9378	0.9304
<i>WGEW</i>				
Maximum aerosol optical depth	0.1887	0.1740	0.1615	0.1431
Minimum aerosol optical depth	0.0851	0.0797	0.0750	0.0575
Maximum Rayleigh optical depth	0.1366	0.0711	0.0392	0.0150
Minimum Rayleigh optical depth	0.1340	0.0698	0.0385	0.0147
Maximum gaseous transmittance	1.0000	0.9974	0.9891	0.9750
Minimum gaseous transmittance	0.9865	0.9270	0.9454	0.9501

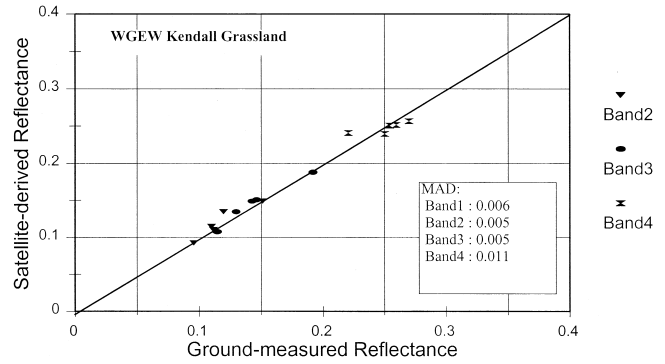


Fig. 7. Values of $\rho_{s\lambda}$ retrieved from the Landsat-5 TM and Landsat-7 ETM+ image using the REL approach compared with ground-based measurements of $\rho_{s\lambda}$ of the Kendall grassland site in WGEW, where Band2, Band3, and Band4 refer to the Landsat-5 TM and Landsat-7 ETM+ spectral bands 2 (green), 3 (red), and 4 (NIR).

dn values listed in Table 3. This resulted in three sets of $\rho_{s\lambda}$ values for the Kendall site: $\rho_{s\lambda AVG}$, $\rho_{s\lambda MIN}$, and $\rho_{s\lambda MAX}$, where $\rho_{s\lambda AVG}$ was computed using values of 40, 13, 10, and 6 for dn for $\rho_{s\lambda} = 0$ in spectral bands 1–4, respectively; $\rho_{s\lambda MIN}$ was computed using values of 31, 11, 8, and 5; and $\rho_{s\lambda MAX}$ was computed using values of 45, 14, 11, and 6. The MADs between $\rho_{s\lambda AVG}$ and $\rho_{s\lambda MIN}$ for the Kendall site on four dates (listed above) were 0.011, 0.005, 0.005, and 0.002 for TM spectral bands 1–4, respectively. For the same site, dates and bands, the MADs between $\rho_{s\lambda AVG}$ and $\rho_{s\lambda MAX}$ were 0.007, 0.003, 0.002, and 0.000. This limited sensitivity test illustrated that for a relatively bright site ($\rho_{s\lambda} = 0.10–0.28$), a reasonable selection of values of dn for $\rho_{s\lambda} = 0$ resulted in $\rho_{s\lambda}$ precision of ranging from about $\rho_{s\lambda} = 0.01$ for TM spectral band 1 to $\rho_{s\lambda} = 0.001$ for TM spectral band 4. This order-of-magnitude difference in precision between spectral bands in the blue and NIR spectrum is due primarily to the greater scattering of light in the shorter visible wavelengths resulting in a potentially greater range of values of dn for $\rho_{s\lambda} = 0$. Thus, the sensitivity of the REL approach to the selection of the dn for $\rho_{s\lambda} = 0$ will be greater for shorter wavelengths. This sensitivity will also increase as the target $\rho_{s\lambda}$ approaches zero because the accuracy of the dn for $\rho_{s\lambda} = 0$ will have greater influence on retrieved $\rho_{s\lambda}$ than the accuracy of the bright target $\rho_{s\lambda}$ (see Fig. 1).

5. Conclusions and summary

The REL approach allows RFR based on a relation between dn and $\rho_{s\lambda}$ derived from two points: a single high-reflectance target within the scene and an estimate of the image dn that would be associated with a surface of $\rho_{s\lambda} = 0$. This approach is particularly suitable for RFR from long-term image sets such as those produced by the Landsat TM and ETM+ sensors over the past 18 years and those to be produced

for years to come. The REL approach requires (1) one large, stable, high-reflectance target within the scene, (2) a measurement of the BRDF of this target, and (3) an estimate of dn for $\rho_{s\lambda}=0$ derived from an RTM using rough estimates of atmospheric conditions. The advantage of REL over most EL approaches is that only one within-scene calibration target is required and that target need not necessarily be flat, homogeneous, vegetation-free nor Lambertian.

This study has shown that there are a variety of bright targets that meet the size and brightness requirements for the REL approach. The suitability of the target can be quantified by determining the residual of measured $\rho_{s\lambda}$ and $\rho_{s\lambda}$ modeled with a BRDF equation similar to Eq. (1) or Eq. (2). The inclusion of BRDF characterization of the calibration targets is a simple but important step in the REL approach. It is apparent from the data reported in Fig. 2 that variation in $\rho_{s\lambda}$ associated simply with θ_s can be as large as 0.10 over a reasonable range of θ_s . In this report, a half-day measurement protocol is suggested that can be used to determine the target BRDF and thus minimize the large potential error in estimation of target $\rho_{s\lambda}$.

As part of this study, values of dn for $\rho_{s\lambda}=0$ were derived for Landsat-5 TM and Landsat-7 ETM+ for clear sky conditions in Arizona (Table 3). For applications of REL at locations where access to an RTM and/or atmospheric measurements is limited, these dn could be used as a baseline. That is, the dn reported in Table 3 could be used for REL with the assumption that these are values for a relatively clear and exceptionally dry atmosphere and thus the REL image conversion would rarely overestimate the effects of atmospheric conditions at other sites.

This study showed that the REL approach worked well for a 10-year Landsat-5 TM and Landsat-7 ETM+ image set at WGEW in Arizona and $\rho_{s\lambda}$ was retrieved with an estimated accuracy of 0.01. Future studies should be focused on repeated validation of the REL approach at other locations and further sensitivity analysis to determine the required accuracy of the target BRDF and the estimation of dn for $\rho_{s\lambda}=0$.

Acknowledgments

This work was made possible by the generous funding and support of the NASA Landsat7 Science Team (NASA S-41396-f) and the encouragement of Drs. Darrel Williams, Sam Goward, and Jim Irons. Some of the aircraft-based reflectance measurements were provided by the scientists, engineers, and pilots from the NASA Stennis Space Flight Center, Utah State University, and University of Arizona. This work was greatly assisted by funding from the University of Córdoba, Department of Agricultural Engineering, Córdoba, Spain, and the encouragement of Drs. Juan Vicente Giraldez, Luciano Mateos, and Elias Fererez. As always, the staff at the USDA Agricultural Research Service Walnut Gulch Experimental Watershed and the

University of Arizona Maricopa Agricultural Center were critical to the successful field experiments.

References

- Biggar, S. F., Gellman, D. I., & Slater, P. N. (1990). Improved evaluation of optical depth components from Langley plot data. *Remote Sensing of Environment*, 32, 91–101.
- Caselles, V., & López García, M. J. (1989). An alternative simple approach to estimate atmospheric correction in multitemporal studies. *International Journal of Remote Sensing*, 10, 1127–1134.
- Freemantle, J. R., Pu, R., & Miller, J. R. (1992). Calibration of imaging spectrometer data to reflectance using pseudo-invariant features. In: *Proceedings of the 15th Canadian symposium on remote sensing, Toronto, Canada* (pp. 452–455).
- Goodrich, D. C., Chehbouni, A., Goff, B., MacNish, B., Maddock, T., Moran, M. S., Shuttleworth, W. J., Williams, D. G., Watts, C., Hipps, L. H., Cooper, D. I., Schieldge, J., Kerr, Y. H., Arias, H., Kirkland, M., Carlos, R., Cayrol, P., Kepner, W., Jones, B., Avissar, R., Begue, A., Bonnefond, J. -M., Boulet, G., Brannan, B., Brunel, J. P., Chen, L. C., Clarke, T., Davis, M. R., DeBruin, H., Dedieu, G., Elguero, E., Eichinger, W. E., Everitt, J., Garatuza-Payan, J., Gempko, V. L., Gupta, H., Harlow, C., Hartogensis, O., Helfert, M., Holifield, C., Hymer, D., Kahle, A., Keefer, T., Krishnamoorthy, S., Lhomme, J. -P., Lagouarde, J. -P., Lo Seen, D., Luquet, D., Marsset, R., Monteny, B., Ni, W., Nouvellon, Y., Pinker, R., Peters, C., Pool, D., Qi, J., Rambal, S., Rodriguez, J., Santiago, F., Sano, E., Schaeffer, S. M., Schulte, M., Scott, R., Shao, X., Snyder, K. A., Sorooshian, S., Unkrich, C. L., Whitaker, M., Yucel, I. (2000). Preface Paper to the Semi-Arid Land-Surface-Atmosphere (SALSA) Program Special Issue. *Agricultural and Forest Meteorology*, 105, 3–20.
- Herman, B. M., & Browning, S. R. (1965). A numerical solution to the equation of radiative transfer. *Journal of the Atmospheric Sciences*, 22, 59–66.
- Jackson, R. D. (1990). The MAC experiments. *Remote Sensing of Environment*, 32, 77–79.
- Jackson, R. D., Moran, M. S., Slater, P. N., & Biggar, S. F. (1987). Field calibration of reference reflectance panels. *Remote Sensing of Environment*, 22, 145–158.
- Jackson, R. D., Teillet, P. M., Slater, P. N., Fedesojevs, G., Jasinski, M. F., Aase, J. K., & Moran, M. S. (1990). Bidirectional measurements of surface reflectance for view angle corrections of oblique imagery. *Remote Sensing of Environment*, 32, 189–202.
- Jacquemund, S., Baret, F., & Hanocq, J. F. (1992). Modeling spectral and bidirectional soil reflectance. *Remote Sensing of Environment*, 41, 123–132.
- Kustas, W. P., & Goodrich, D. C. (1994). Preface: Monsoon'90 multidisciplinary experiment. *Water Resources Research*, 30, 1211–1225.
- McCardle, S. S., Miller, J. R., & Freemantle, J. R. (1992). Airborne image acquisition under cloud: preliminary comparisons with clear-sky scene radiance and reflectance imagery. In: *Proceedings of the 15th Canadian symposium on remote sensing, Toronto, Canada* (pp. 446–449).
- Moran, M. S., Clarke, T. R., Qi, J., Barnes, E. M., & Pinter, P. J. Jr. (1997). Practical techniques for conversion of airborne imagery to reflectances. In: *16th Biennial workshop on color photography and videography in research assessment, Weslaco, TX*, (pp. 82–95) April 29–May 1.
- Moran, M. S., Clarke, T. R., Qi, J., & Pinter, P. J. Jr. (1996). MAD-MAC: a test of multispectral airborne imagery as a farm management tool. In: *Proceedings of the 26th international symposium on remote sensing of environment, Vancouver, BC, Canada*, (pp. 612–617) March 25–29.
- Moran, M. S., Goodrich, D. C., & Kustas, W. P. (1994). Integration of remote sensing and hydrologic modeling through multi-disciplinary semiarid field campaigns: Monsoon'90, Walnut Gulch'92 and SAL-

- SA-MEX. In: *Proceedings of the 6th international symposium on physical measures and signatures in remote sensing, Val d'Isere, France*, (pp. 981–991) January 17–21.
- Moran, M. S., Jackson, R. D., Clarke, T. R., Qi, J., Cabot, F., Thome, K. J., & Markham, B. L. (1995). Reflectance factor retrieval from Landsat TM and SPOT HRV data for bright and dark targets. *Remote Sensing of Environment*, 52, 218–230.
- Moran, M. S., Jackson, R. D., Slater, P. N., & Teillet, P. M. (1992). Evaluation of simplified procedures for retrieval of land surface reflectance factors from satellite sensor output. *Remote Sensing of Environment*, 41, 169–184.
- Moran, M. S., Qi, J., Ni, W., & Shannon, D. T. (2000). Water Conservation Laboratory image and ground data archive (WIGDA99) for Arizona agricultural and rangeland regions. In: *Second international conference on geospatial information in agric. and for., Orlando, FL*, (pp. II 229–II 236) January 10–12.
- Nilson, T., & Kuusk, A. (1989). A reflectance model for the homogeneous plant canopy and its inversion. *Remote Sensing of Environment*, 27, 157–167.
- Qi, J., Cabot, F., Moran, M. S., Dedieu, G., & Thome, K. J. (1995). Biophysical parameter retrievals using multidirectional measurements. *Remote Sensing of Environment*, 54, 71–83.
- Qi, J., Moran, M. S., Cabot, F., & Dedieu, G. (1995). Normalization of sun/view angle effects on vegetation indices with bidirectional reflectance function models. *Remote Sensing of Environment*, 52, 207–217.
- Rahman, H., & Dedieu, G. (1994). A simplified method for the atmospheric correction of satellite measurements in the solar spectrum. *International Journal of Remote Sensing*, 15, 123–143.
- Renard, K. G., Lane, L. J., Simanton, J. R., Emmerich, W. E., Stone, J. J., Weltz, M. A., Goodrich, D. C., & Yakowitz, D. S. (1993). Agricultural impacts in an arid environment: Walnut Gulch case study. *Hydrological Sciences Technology*, 9, 145–190.
- Schott, J. R., Salvaggio, C., & Volchok, W. J. (1988). Radiometric scene normalization using pseudoinvariant features. *Remote Sensing of Environment*, 26, 1–16.
- Slater, P. N. (1980). *Remote sensing: optics and optical systems*. Reading, MA: Addison-Wesley Publishing (575 pp.).
- Slater, P. N., Biggar, S. F., Holm, R. G., Jackson, R. D., Mao, Y., Moran, M. M., Palmer, J. M., & Yuan, B. (1987). Reflectance- and radiance-based methods for the in-flight absolute calibration of multispectral sensors. *Remote Sensing of Environment*, 22, 11–37.
- Slater, P. N., & Jackson, R. D. (1982). Atmospheric effects on radiation reflected from soil and vegetation as measured by orbital sensors using various scanning directions. *Applied Optics*, 21, 3923–3931.
- Smith, G. M., & Milton, E. J. (1999). The use of the empirical line method to calibrate remotely sensed data to reflectance. *International Journal of Remote Sensing*, 20, 2653–2662.
- Tanré, D., Deroo, C., Duhaut, P., Herman, M., Morcette, J. J., Perbos, J., & Deschamps, P. Y. (1990). Description of a computer code to simulate the satellite signal in the solar spectrum: the 5S code. *International Journal of Remote Sensing*, 11, 659–668.
- Teillet, P. M., & Fedosejevs, G. (1995). On the dark target approach to atmospheric correction of remotely sensed data. *Canadian Journal of Remote Sensing*, 21, 374–387.
- Thome, K. Absolute radiometric calibration of Landsat-7 ETM+ using the reflectance based method. *Remote Sensing of Environment*, 78, 27–38.
- Thome, K. J., Gellman, D. I., Parada, R. J., Biggar, S. F., Slater, P. N., & Moran, M. S. (1993). In-flight radiometric calibration of Landsat-5 Thematic Mapper from 1984 to present. In: *Proceedings of the Society of Photo-Optical Instruments and Engineering symposium, Orlando, FL*, (pp. 126–130) April 12–16.
- Walthall, C. L., Norman, J. M., Welles, J. M., Campbell, G., & Blad, B. L. (1985). Simple equation to approximate the bidirectional reflectance from vegetative canopies and bare soil surfaces. *Applied Optics*, 24, 383–387.